Lecture Notes in Mobility

Tim Schulze
Beate Müller
Gereon Meyer *Editors*

Advanced Microsystems for Automotive Applications 2016

Smart Systems for the Automobile of the Future

EPoSS
European Technology Platform
on Smart Systems Integration

VDI | VDE | IT

Springer

Lecture Notes in Mobility

Series editor

Gereon Meyer, Berlin, Germany

More information about this series at http://www.springer.com/series/11573

Tim Schulze · Beate Müller
Gereon Meyer
Editors

Advanced Microsystems for Automotive Applications 2016

Smart Systems for the Automobile of the Future

Springer

Editors
Tim Schulze
VDI/VDE Innovation + Technik GmbH
Berlin
Germany

Gereon Meyer
VDI/VDE Innovation + Technik GmbH
Berlin
Germany

Beate Müller
VDI/VDE Innovation + Technik GmbH
Berlin
Germany

ISSN 2196-5544 ISSN 2196-5552 (electronic)
Lecture Notes in Mobility
ISBN 978-3-319-44765-0 ISBN 978-3-319-44766-7 (eBook)
DOI 10.1007/978-3-319-44766-7

Library of Congress Control Number: 2016947919

Printed on acid-free paper

This Springer imprint is published by Springer Nature
The registered company is Springer International Publishing AG
The registered company address is: Gewerbestrasse 11, 6330 Cham, Switzerland

Preface

Automated vehicles are currently raising considerable attention of politics and industry alike. Although public funding of research and innovation on automated driving dates back as far as the 1980s, interest has been peaking very recently following the demonstration of advanced technologies by key players that seemingly is at the verge of market-readiness. In effect, fierce competition is unfolding between companies regarding the enabling technologies like sensors, powerful automotive ECUs and actuators. At the same time, governments are debating on the legal and infrastructural preconditions of automated driving and about how to harmonize the necessary investments. Yet, the recent first fatal incident with a beta-state self-driving vehicle remind us that the current technology is not yet capable of mastering all complex situations.

The current developments imply two major challenges: Firstly, research and innovation efforts need to be shifted from proof-of-concept to proof-of-safety on the system level of automated driving technology. For instance, the performance envelope of sensors, data fusion and object recognition systems has been pushed considerably in recent years, but does still not cover the complexity that a vehicle encounters in everyday life. Particularly for applications in urban environments and at higher levels of automation, perception of the driving environment is a challenging task still to be mastered in a robust fashion. Smart systems integration that applies a variety of vehicle and infrastructure based sensor systems and finally links it with big data analytics in the cloud will play an important role in this domain, with safety aspects as well as validation methodology becoming a prominent future focus.

Secondly, it is obvious that the economically viable large-scale rollout of driving automation requires involvement and agreement between a large and heterogeneous group of stakeholders encompassing the automotive, IT and telecom sectors as well as road infrastructure providers and public authorities. To this end, a first initiative was launched in Sept. 2015 by Commissioner Oettinger with the Round Table Automated Driving. The recently started Coordination and Support Action "Safe and Connected Automation of Road Transport (SCOUT)" will develop a

cross-sectorial roadmap regarding the implementation of high-degree automated driving in Europe, which will assist the ambition of the roundtable and may serve as a blueprint for research and innovation planning and regulatory actions in the coming years.

The International Forum on Advanced Microsystems for Automotive Applications (AMAA) has been exploring the technological foundations of connected, automated and electrified vehicles for many years. Consequently, the topic of this year's 20th anniversary edition of AMAA, held in Brussels on 22–23 September 2016, is "Smart Systems for the Automobile of the Future". The AMAA organisers, Berlin-based VDI/VDE Innovation + Technik GmbH together with the European Technology Platform on Smart Systems Integration (EPoSS), greatly acknowledge the support given for this conference, particularly from the European Union through the Coordination Actions "Safe and Connected Automation of Road Transport (SCOUT)" and "Action Plan for the Future of Mobility in Europe (Mobility4EU)".

The papers in this book, a volume of the Lecture Notes in Mobility book series by Springer, were written by leading engineers and researchers who have attended the AMAA 2016 conference to report their recent progress in research and innovation. The papers were selected by the members of the AMAA Steering Committee and are made accessible worldwide. As the organisers and the chairman of the AMAA 2016, we would like to express our great appreciation to all the authors for their high-quality contributions to the conference and also to this book. We would also like to gratefully acknowledge the tremendous support we have received from our colleagues at VDI/VDE-IT.

Berlin, Germany
August 2016

Tim Schulze
Beate Müller
Gereon Meyer

Supporters and Organisers

Funding Authority
European Commission

Supporting Organisations
European Council for Automotive R&D (EUCAR)
European Association of Automotive Suppliers (CLEPA)
Strategy Board Automobile Future (eNOVA)
Advanced Driver Assistance Systems in Europe (ADASE)
Zentralverband Elektrotechnik- und Elektronikindustrie e.V. (ZVEI)
Mikrosystemtechnik Baden-Württemberg e.V.

Organisers
European Technology Platform on Smart Systems Integration (EPoSS)
VDI/VDE Innovation + Technik GmbH

Steering Committee

Mike Babala, TRW Automotive, Livonia, MI, USA
Serge Boverie, Continental AG, Toulouse, France
Geoff Callow, Technical & Engineering Consulting, London, UK
Kay Fürstenberg, Sick AG, Hamburg, Germany
Wolfgang Gessner, VDI/VDE-IT, Berlin, Germany
Roger Grace, Roger Grace Associates, Naples, FL, USA
Klaus Gresser, BMW Forschung und Technik GmbH, Munich, Germany
Riccardo Groppo, Ideas & Motion, Cavallermaggiore, Italy
Hannu Laatikainen, Murata Electronics Oy, Vantaa, Finland
Jochen Langheim, ST Microelectronics, Paris, France
Günter Lugert, Siemens AG, Munich, Germany
Steffen Müller, NXP Semiconductors, Hamburg, Germany
Roland Müller-Fiedler, Robert Bosch GmbH, Stuttgart, Germany
Andy Noble, Ricardo Consulting Engineers Ltd., Shoreham-by-Sea, UK
Pietro Perlo, IFEVS, Sommariva del Bosco, Italy
Christian Rousseau, Renault SA, Guyancourt, France
Jürgen Valldorf, VDI/VDE-IT, Berlin, Germany
David Ward, MIRA Ltd., Nuneaton, UK

Conference Chair:
Gereon Meyer, VDI/VDE-IT, Berlin, Germany

Contents

Part I
Networked Vehicles & Navigation

Requirements and Evaluation of a Smartphone Based Dead Reckoning Pedestrian Localization for Vehicle Safety Applications

Johannes Rünz, Folko Flehmig, Wolfgang Rosenstiel and Michael Knoop

Abstract The objective of this paper is to propose a smartphone based outdoor dead reckoning localization solution, show its experimental performance and classify this performance into the context of Vehicle-to-X (V2X) based pedestrian protection systems for vehicle safety applications. The proposed approach estimates the position, velocity and orientation with inertial measurement unit (IMU) sensors, a global navigation satellite system (GNSS) receiver and an air pressure sensor without any restriction to pedestrians, like step length models or a relationship between smartphone orientation and walking direction. Thus, an application makes sense in handbags, trouser pockets or school bags. The dead reckoning localization filter was evaluated in measurements and compared with a highly accurate reference system. Furthermore, the requirements of measurement and modelling uncertainties in a pedestrian protection system with a low false-positive rate were derived and compared with the reference measurements. The results demonstrated that an appropriate use of the proposed system approach is only possible with more accurate positioning solutions from the GNSS receiver. According to this the necessity of differential GNSS methods was predicted.

J. Rünz (✉) · F. Flehmig · M. Knoop
Chassis Systems Control, Robert Bosch GmbH,
Robert-Bosch-Allee 1, 74232 Abstatt, Baden-Württemberg, Germany
e-mail: johannes.ruenz@de.bosch.com

F. Flehmig
e-mail: folko.flehmig@de.bosch.com

M. Knoop
e-mail: michael.knoop@de.bosch.com

W. Rosenstiel
Computer Engineering Department, Eberhard Karls Universität Tübingen,
Auf der Morgenstelle 8, 72076 Tübingen, Baden-Württemberg, Germany
e-mail: rosenstiel@informatik.uni-tuebingen.de

M. Knoop
Institute of Measurement and Control, Karlsruhe Institute of Technology,
Karlsruhe, Germany

T. Schulze et al. (eds.), *Advanced Microsystems for Automotive Applications 2016*, Lecture Notes in Mobility, DOI 10.1007/978-3-319-44766-7_1

Keywords Smartphone based pedestrian protection · Pedestrian dead reckoning · Vehicle safety

1 Introduction

To improve advanced pedestrian protection systems in future vehicles, it is necessary to obtain better knowledge about the pedestrian behavior and the perception to recognize pedestrians in the vehicle's environment [1]. Situations which include visually obstructed pedestrians or pedestrians that cannot be detected by the limited field of view (e.g. in curves), are especially challenging. A possible solution is the cooperative usage of the pedestrian's smartphone with its internal localization sensors and V2X technology to better protect the pedestrian. Besides, the modeling of the pedestrian's intention and behavior might be supported by information from the smartphone. General analysis about the possible system architectures, communication strategies as well as limitations and feasible benefits of pedestrians' smartphones as cooperative sensors are described in [2–5]. Moreover, an experimental proof of benefit for safety applications with bicycles using their smartphones is presented in [6]. The author states that the accuracy of the smartphone's global navigation satellite system (GNSS) receiver is improved with a map-matching algorithm and context knowledge.

As later described in this work, the requested low false-positive rates of pedestrian protection systems lead to strict requirements on the position accuracy of the pedestrian. A survey is given in [7], which shows the accuracy of smartphone GNSS sensors and compares them with a Differential GNSS (DGNSS) system. According to [8], the GNSS sensor is combined with a velocity and orientation estimation through step detection, a gyroscope and a magnetic field sensor in order to further improve the localization performance. A similar approach to improve the GNSS measurements in outdoor environments is used by [9]. The challenge of such approaches is that the orientation of the smartphone must be rigidly coupled with the walking direction, which is not given in its daily use. Thus, the sensor data fusion can deteriorate the accuracy of the GNSS measurements in wrong use cases.

Typical localization problems occur in the field of aerospace engineering with six degrees of freedom: three position and three orientation dimensions. In these surroundings, highly accurate acceleration sensors and gyroscopes are used to derive the position, velocity and orientation of an object. Furthermore in inertial navigation systems (INS) the determined position, velocity and orientation are corrected by GNSS measurements with e.g. a Kalman filter (KF). In [10] implementations of such systems are presented. These methods are then adopted to a drone equipped with MEMS acceleration and gyroscope sensors in [11].

In this work, methods from aerospace engineering are evaluated for INS by using the smartphone's internal sensors. The ambition is to show the localization performance of such a system and classify the results in the context of vehicle safety applications for pedestrians.

First, in Sect. 2 the dead reckoning localization filter structure with its propagation and observation models is described. Furthermore, in Sect. 3 the evaluation procedure with its measurement setup is presented. Finally, Sect. 4 shows the performance of the considered localization filter and classifies the results into the context of pedestrian protection systems.

2 Localization Estimation Filter

In this work, a general approach from the aerospace engineering described in [10, 11], without assumptions about the relationship between walking direction and smartphone orientation or step length, is used. In aerospace engineering, a filter that estimates the position, velocity and orientation, is called *navigation filter*. Because of the different meaning of "navigation" in the vehicle context, these filters will be called localization filters in this paper.

Figure 1 shows the reduced structure of the estimation filter. The output of the dead reckoning estimation filter consists of the estimated position $\hat{\boldsymbol{p}}^n_{bn}$, the estimated velocity $\hat{\boldsymbol{v}}^n_{bn}$ and the estimated orientation $\hat{\boldsymbol{q}}^n_{bn}$ given in quaternion representation. As inputs, an inertial measurement unit (IMU) with its measurements $\boldsymbol{f}^b_{ib}$ and $\boldsymbol{\omega}^b_{ib}$, a GNSS receiver and a barometer are used.

To propagate the position, velocity and orientation with an IMU two different methods are known. First the acceleration sensors can be mounted on a Gyro-stabilized gimbal platform, which leads to a fixed orientation of the acceleration sensors, to the earth. The other method is, that the acceleration is rigidly coupled with the body ("strap-down"), which leads to a more complex problem to interpret the measurements. The *strapdown algorithm* determines the updated position $\hat{\boldsymbol{p}}^n_{bn}$, velocity $\hat{\boldsymbol{v}}^n_{bn}$ and orientation $\hat{\boldsymbol{q}}^n_{bn}$ with the corrected measurements $\boldsymbol{f}^b_{ib}$

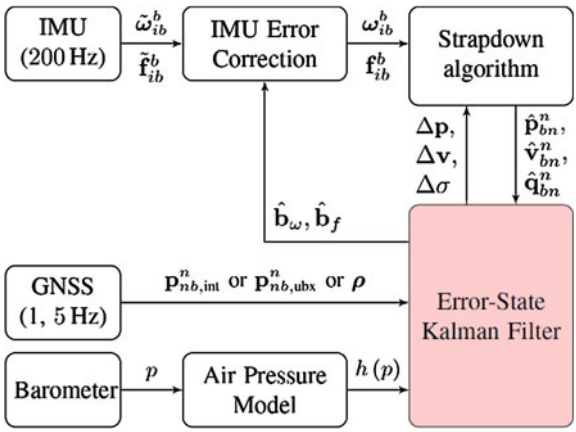

Fig. 1 Schematic representation of the localization filter structure

and $\boldsymbol{\omega}_{ib}^{b}$ from the rigidly coupled acceleration sensor and gyroscope of the smartphone. This is done by three integration steps and compensation of parasitic influences like the measured earth gravity. Because of the noncommutativity of rotations and the Nyquist Shannon theorem, the strapdown algorithm is sampled with a high frequency of 200 Hz. As a consequence of the strapdown algorithm, the measured acceleration in and the rotation rate around the navigation coordinate system axis (east-, north- and up-axis) can be directly determined. To have a long term stability and accuracy, the estimated values must be corrected with absolute position measurements. Therefore, an extended error-state KF uses GNSS and barometric pressure measurements to estimate the position errors $\Delta\boldsymbol{p}$, velocity errors $\Delta\boldsymbol{v}$ and orientation errors $\Delta\boldsymbol{\sigma}$, which are used to correct the absolute states $\hat{\boldsymbol{p}}_{bn}^{n}$, $\hat{\boldsymbol{v}}_{bn}^{n}$ and $\hat{\boldsymbol{q}}_{bn}^{n}$. Furthermore, the KF estimates the parameters $\boldsymbol{b}_{\omega}$ and $\boldsymbol{b}_{f}$ of the measurement error models.

It is also possible to observe the orientation with a magnetic field sensor and earth magnetic field assumption. Due to unpredictable disturbances by ferromagnetic materials in the environment, like vehicles, this method is not used in this paper.

In the following, the sensor error models, the propagation error-state model and the observations for correcting the KF error-state are presented.

2.1 Sensor Error Models and Impact of the Error Terms

The acceleration sensor should measure the specific force $\boldsymbol{f}_{ib}^{b}$ while the gyro measures the rotation rate $\boldsymbol{\omega}_{ib}^{b}$. The smartphone microelectromechanical systems (MEMS) sensors have time-variant bias sensor errors $\hat{\boldsymbol{b}}_{\omega}$ and $\hat{\boldsymbol{b}}_{f}$, which must be estimated by the KF. Furthermore, there are scaling errors $\hat{\boldsymbol{s}}_{\omega}$ and $\hat{\boldsymbol{s}}_{f}$, that are assumed as time-invariant. The error models are then given by

$$\boldsymbol{\omega}_{ib}^{b} = \mathrm{diag}(\hat{\boldsymbol{s}}_{\omega})\tilde{\boldsymbol{\omega}}_{ib}^{b} + \hat{\boldsymbol{b}}_{\omega} \quad \text{and} \tag{1}$$

$$\boldsymbol{f}_{ib}^{b} = \mathrm{diag}\left(\hat{\boldsymbol{s}}_{f}\right)\tilde{\boldsymbol{f}}_{ib}^{b} + \hat{\boldsymbol{b}}_{f}. \tag{2}$$

In this work, misalignment errors of the assembled IMU sensors are neglected.

The time-variant bias errors of MEMS IMUs lead to significant errors in the position propagation with the strapdown algorithm. Especially bias errors of the gyroscope result in wrong orientations that couple the gravity acceleration into the two integration steps for position determination. For this reason the performance of the strapdown algorithm is highly dependent on the bias errors estimation accuracy.

2.2 Error-State Model

The model has the error-state vector

$$\boldsymbol{x} = \left(\Delta\boldsymbol{p}, \Delta\boldsymbol{v}, \Delta\boldsymbol{\sigma}, \Delta\boldsymbol{b}_{\omega}, \Delta\boldsymbol{b}_{f}, \Delta c\boldsymbol{T}\right)^{T}, \tag{3}$$

where $\Delta\boldsymbol{b}_{\omega}$ and $\Delta\boldsymbol{b}_{f}$ are the errors of the IMU biases and

$$\Delta c\boldsymbol{T} = c(\delta \mathrm{t}_{\mathrm{rec}}, \delta \dot{t}_{rec})$$

is the GNSS receiver's clock error δt_{rec} and its drift $\delta \dot{t}_{rec}$, which are essential to consider the raw measurements of the GNSS receiver. The error propagation model is in-depth derived in [11] and given in its continuous form by

$$\dot{\boldsymbol{x}} = \begin{pmatrix} \mathbf{0} & \boldsymbol{I} & \mathbf{0} & \mathbf{0} & \mathbf{0} & \mathbf{0} \\ \mathbf{0} & \mathbf{0} & -(\boldsymbol{C}_{b}^{\hat{n}}\boldsymbol{f}_{ib}^{i}\times) & -\boldsymbol{C}_{b}^{\hat{n}} & \mathbf{0} & \mathbf{0} \\ \mathbf{0} & \mathbf{0} & \mathbf{0} & \mathbf{0} & -\boldsymbol{C}_{b}^{\hat{n}} & \mathbf{0} \\ \mathbf{0} & \mathbf{0} & \mathbf{0} & \mathbf{0} & \mathbf{0} & \mathbf{0} \\ \mathbf{0} & \mathbf{0} & \mathbf{0} & \mathbf{0} & \mathbf{0} & \mathbf{0} \\ \mathbf{0} & \mathbf{0} & \mathbf{0} & \mathbf{0} & \mathbf{0} & \boldsymbol{F}_{\Delta c\boldsymbol{T}} \end{pmatrix} \boldsymbol{x}, \tag{4}$$

where $\boldsymbol{I}$ is the 3×3 identity matrix, $\boldsymbol{C}_{b}^{\hat{n}}$ is the direct cosine matrix to rotate the IMU coordinates to the estimated navigation frame, $\boldsymbol{f}_{ib}^{i}\times$ is the skew-symmetric matrix representation of the vector cross product of $\boldsymbol{f}_{ib}^{i}$ and $\boldsymbol{F}_{\Delta cT}$ is given by

$$\boldsymbol{F}_{\Delta cT} = \begin{pmatrix} 0 & 1 \\ 0 & 0 \end{pmatrix}. \tag{5}$$

The absolute states are always corrected with the estimated errors after every observation step of the KF. Afterwards, the error-states are reset to zero, so that a nonlinear error propagation is not necessary.

2.3 Observation Models

For correcting the determined position, velocity and orientation of the strapdown algorithm, the measurements of a GNSS receiver and a barometer are used.

Internally, a GNSS receiver measures the geometric distances to the satellites which are summed up with other error terms. In particular the clock error $c\boldsymbol{T}$ of the GNSS receiver produces a significant error. The measurement of the geometric distance, added by the clock error term, is referred to as pseudorange $\tilde{\rho}_i$ of satellite i. From a set of pseudoranges of different satellites, the GNSS receiver's position solution $\tilde{\boldsymbol{p}}_{GNSS}^{n}$ can be deduced.

In a localization filter, either the pseudoranges in a *tightly coupled filter* concept or the position solution in a *loosely coupled filter* concept can be used to improve the estimation. In the next sections, the different observation matrixes are presented.

2.3.1 Loosely Coupled GNSS Measurement

In a loosely coupled filter the position solution $\tilde{\boldsymbol{p}}^n_{GNSS}$ GNSS is used as an observation for the KF's correction step. The observation matrix $\boldsymbol{H}_{p,GNSS}$ is given in [11] by

$$\boldsymbol{H}_{p,GNSS} = (\boldsymbol{I} \quad \boldsymbol{0} \quad \boldsymbol{0} \quad \boldsymbol{0} \quad \boldsymbol{0} \quad \boldsymbol{0}), \tag{6}$$

where $\boldsymbol{I}$ is a 3×3 identity matrix and $\boldsymbol{0}$ are zero matrices. The advantage of using the position solution is the availability in every GNSS receiver and the low calculation effort as compared to a tightly coupled system.

2.3.2 Tightly Coupled GNSS Measurement

The tightly coupled observation matrix $\boldsymbol{H}_{\rho_i}$ is given by

$$\boldsymbol{H}_{\rho_i} = \begin{pmatrix} \boldsymbol{e}^n_{Sat,i} & \boldsymbol{0} & \boldsymbol{0} & \boldsymbol{0} & 1 & 0 \end{pmatrix} \text{ with} \tag{7}$$

$$\boldsymbol{e}^n_{Sat,i} = \frac{-(\boldsymbol{p}^n_{Sat,i} - \boldsymbol{p}^n_{bn})}{\sqrt{\left(\boldsymbol{p}^n_{Sat,i} - \boldsymbol{p}^n_{bn}\right)^T (\boldsymbol{p}^n_{Sat,i} - \boldsymbol{p}^n_{bn})}}. \tag{8}$$

The advantage of this method is that any number of pseudoranges helps to improve the absolute position accuracy of the localization filter, whereas the loosely coupled system typically needs four satellites to determine a position solution. Furthermore, the handling with obvious measurement errors is easier with the isolated pseudorange measurements.

2.3.3 Barometric Height Measurement

With the barometric formula

$$p(h) = p(h_0) \exp\left(-\frac{Mg\Delta h}{RT}\right), \tag{9}$$

with $p(h_0)$ is the static pressure, M is the molar mass of Earth's air, g gravitational acceleration, R universal gas constant for air, T is the standard temperature and Δh is the height difference to the height h_0, the observation matrix $\boldsymbol{H}_{\rho_u}$ can be derived to

$$\boldsymbol{H}_{\rho_u} = \left(0 \quad 0 \quad p(h_0)\frac{Mg\Delta h}{RT}\exp\left(-\frac{Mg\Delta h}{RT}\right) \quad \mathbf{0} \quad \ldots \quad \mathbf{0}\right). \tag{10}$$

To get consistent height measurements with the GNSS measurements, it is necessary to adopt the static pressure $p(h_0)$ online.

3 Methods

The presented localization filter was implemented on a Samsung Galaxy S3. In order to examine also a tightly coupled INS and the additional benefit of a more accurate GNSS receiver a commercial *u-blox M8N* receiver is connected to the smartphone by USB OTG.

The KF is implemented according to the numerical stable Bierman-Thronton [12] method. The scaling errors $\hat{\boldsymbol{s}}_\omega$ and $\hat{\boldsymbol{s}}_f$ are assumed to be time-invariant and are determined in a special calibration process before the measurements.

3.1 Reference Measurement System

The experiments were carried out with the setup shown in Fig. 2. A highly accurate GeneSys ADMA-G was used to give a reference. The ADMA-G can be mounted on the back of a pedestrian together with the GNSS antenna and the GSM receiver unit for DGPS corrections. Optionally, a smartphone can be mounted on a dedicated area to obtain a fixed orientation between the smartphone and the ADMA-G.

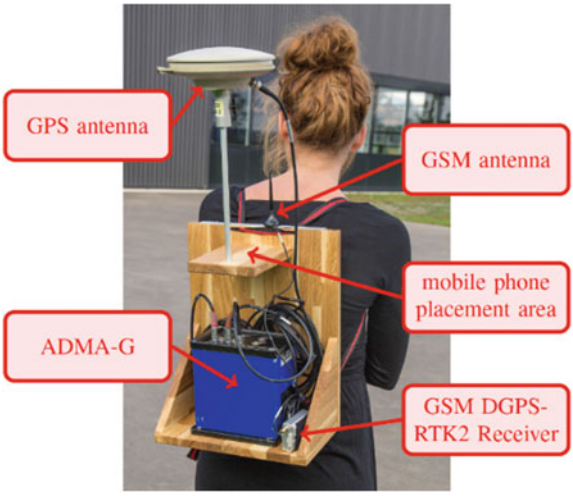

Fig. 2 Reference measurement setup with a high accuracy INS-System ADMA-G with closed-loop fiber-optic gyroscope and servo accelerometers

Table 1 Major differences between reference system GeneSys ADMA-G and smartphone sensors

	Smartphone	ADMA-G
Gyroscope type	MEMS	Closed-loop fiber gyroscope
Acceleration type	MEMS	3 servo accelerometers
GPS type	Single L1	Single L1, DPS-RTK2
Gyroscope accuracy	$\pm 250\,°\mathrm{h}^{-1}$	$1\,°\mathrm{h}^{-1}$
Acceleration accuracy	$\pm$10mg	1mg
Positioning accuracy		1.8 m. . .0.02 m

The ADMA-G itself is also an INS system with highly accurate fiber-optic gyroscope and servo accelerometers. The absolute position corrections are given by a Single L1, DPS-RTK2 GNSS receiver, which permits a position accuracy up to $\sigma_{p,min} = 0.02\,\mathrm{m}$ [13].

Table 1 demonstrates the important differences between the reference and the smartphone INS system. Primarily, the IMU sensors and the accurate DGPS system results in a higher accuracy. The smartphone is assembled with an integrated triaxial accelerometer and triaxial gyroscope of type InvenSense MPU-6500.

To minimize errors in the strapdown algorithm, mainly caused by the non-commutativity of the rotation, it is sampled with a high frequency of 200 Hz. The atmospheric pressure measurements are sampled with 1 Hz because of the low dynamics in height. The smartphone internal GNSS receiver supports a maximal sample frequency of 1 Hz, whereas the external u-blox M8N receiver is sampled with 5 Hz.

3.2 Measurement Environment

The measurements were done in a GNSS friendly environment (no or little multipath effects) on a cloudy day. The ADMA-G asserts a maximal position standard deviation of 0.03 m during the whole considered measurement.

Figure 3 shows the trajectory of the measurement. The pedestrian walks on a slightly curved way and does some 90° turns.

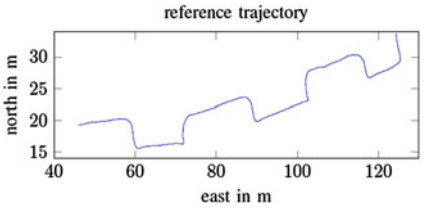

Fig. 3 The considered reference measurement trajectory measured with ADMA-G. The trajectory with some 90° turns was walked within 90 s on a slightly curved way in a GNSS-friendly environment

4 Results

4.1 GNSS Receiver and Method Comparison

Figure 4 shows the horizontal positioning errors of the different localization estimation filters. The best results are achieved with the position solution of the external u-blox M8N GNSS receiver with a RMS error of 0.74 m. The tightly coupled position solution has a RMS error of 1.194 m with the existence of significant outliers in comparison to the u-blox M8N loosely coupled solution. With a RMS error of 1.90 m, the smartphone's internal GNSS achieves the poorest positioning performance.

Due to the sensor data fusion, it is possible to compensate noise of the GNSS receiver with the IMU strapdown propagation. But if the GNSS receiver, like the smartphone's internal GNSS receiver, has got a constant offset compared to the reference, it is impossible to eliminate these errors through sensor data fusion or averaging. To guarantee a better absolute positioning performance it is necessary to have unbiased absolute position measurements e.g. usingDGNSS methods.

4.2 Velocity Accuracy

In particular for cooperative systems, as described in [14], the velocity of the pedestrian is interesting for the situation risk assessment. The position can be determined very quickly through the environment sensors, whereas the velocity must be determined over a few measurements.

With the u-blox M8N GNNS receiver and a loosely coupled localization filter architecture the overall RMS velocity error is 0.13 ms^{-1}. Later in this work, this value is used to assess the situation analysis.

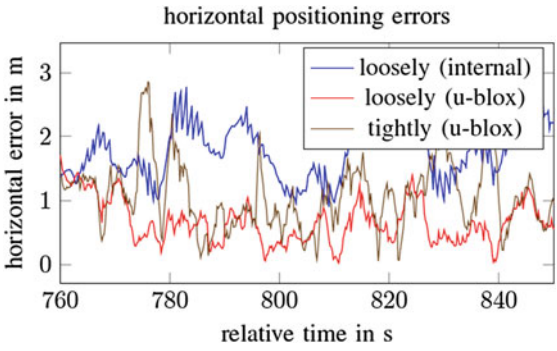

Fig. 4 Horizontal positioning error

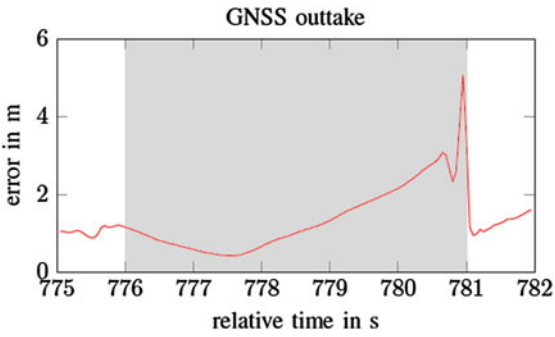

Fig. 5 Horizontal position error in a simulated 5 s GNSS outage during a 90° turn. During the shaded time interval there are no GNSS updates. The position is only determined with the IMU measurements through the strapdown algorithm

4.3 Simulated Short-Time GNSS Outage

In Fig. 5 GNSS outage of 5 s during a 90° turn is simulated. It can be noticed that the positioning error increases in this interval to a value of several meters. Thus, this shows that the IMU of the smartphone can be used for a short-time position prediction between GNSS updates. However, it is not possible to bridge longer GNSS outages or to give a useful position estimation.

The advantage of the strapdown position propagation is the immediate reaction response on changes in motion of the pedestrian. Furthermore, in comparison to the accuracy of [8], it can be observed that with a good GNSS availability the propagation accuracy of smartphone's IMU during a step interval is good enough, so that no further methods, like step detection to improve the velocity estimation, are needed.

4.4 Location Estimation Accuracy Requirements for Pedestrian Protection Systems

The parametrization of advanced driver assistant systems for pedestrian protection is always a compromise between an inadvertent false-positive rate r_{FP} and a required true-positive rate r_{TP} to achieve a system benefit. To determine these rates in a given situation, it is necessary to know the probability P_{FP} of a false-positive event and P_{TP} of a true-positive event. In addition the statistical occurrence rate r_{Sit} of such a situation must be known. This leads to

$$r_{FP} = P_{FP} r_{Sit} \quad \text{and} \tag{10}$$

$$r_{TP} = P_{TP} r_{Sit}. \tag{11}$$

In the following, the false-positive und true-positive probabilities P_{FP} and P_{FP} are analyzed in-depth.

First of all, the behavior of the pedestrian has to be modeled. In general the 2D position trajectory $\boldsymbol{p}_{pred}(t)$ of a pedestrian over a prediction interval $t \in [0, t_{pred}]$ can be expressed by

$$\boldsymbol{p}_{pred}(t) = \boldsymbol{p}_{meas} + t\boldsymbol{v}_{meas} + \int_0^t \int \boldsymbol{a}_{model}(t)dt\,dt, \tag{12}$$

where $\boldsymbol{p}_{meas}$ and $\boldsymbol{v}_{meas}$ are the position and velocity of the measurement, e.g. the localization filter, and $\boldsymbol{a}_{model}(t)$ is the predictive behavior model of the pedestrian. [14, 15] show possibilities to choose the prediction model $\boldsymbol{a}_{model}(t)$. If it is assumed that $\boldsymbol{p}_{meas}$, $\boldsymbol{v}_{meas}$ and $\boldsymbol{a}_{model}(t)$ are binomial normal distributed and time-invariant, the predicted position $\boldsymbol{p}_{pred}(t)$ is also binomial normal distributed with mean $\boldsymbol{\mu}_{pred}(t)$ and covariance $\boldsymbol{\Sigma}_{pred}(t)$

$$\boldsymbol{\mu}_{pred}(t) = \boldsymbol{\mu}_{pred} + t\boldsymbol{\mu}_{v_{meas}} + \frac{t^2}{2}\boldsymbol{\mu}_{a_{model}} \quad \text{and} \tag{13}$$

$$\boldsymbol{\Sigma}_{pred}(t) = \boldsymbol{\Sigma}_{pred} + t^2\boldsymbol{\Sigma}_{v_{meas}} + \frac{t^4}{4}\boldsymbol{\Sigma}_{a_{model}} \tag{14}$$

Based on this information, the front collision probability P_{coll} for a certain prediction time t_{pred} can be calculated as shown in [16]. It must be noted that the uncertainty of position, velocity and orientation of the ego vehicle must be taken into account for determining the collision probability P_{coll}.

In the following, for simplicity, a diagonal covariance matrix $\boldsymbol{\Sigma}_{pred}(t_{TTC}) = \sigma^2\boldsymbol{I}$ is assumed. Figure 6 shows the front collision probability P_{coll} of a pedestrian

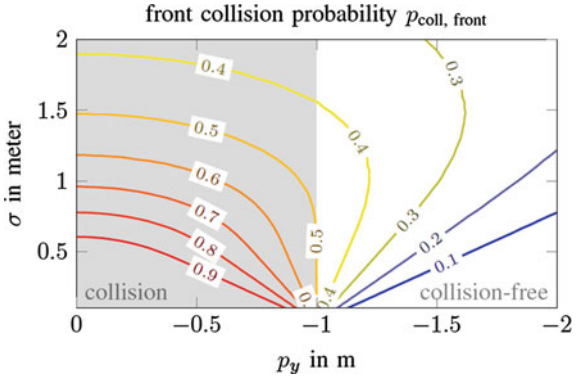

Fig. 6 Front collision probability p_{coll} respects to the standard deviation σ of the position measurement and the pedestrians crossing point p_y of the vehicle front line. It is assumed that the standard deviation σ is not growing with the time. In the shaded area there is a front collision with the vehicle. Only the half vehicle front line is represented with the middle of the vehicle at $p_y = 0\,\text{m}$

which crosses the vehicle front line at a given point p_y with a given standard deviation σ. The vehicle front covers a horizontal-axis from $p_y \in [-1, 1]$. The grey shaded area marks collisions where $p_y = 0\,\text{m}$ means a collision at the middle of the vehicle and $p_y = -1\,\text{m}$ is a collision with the right edge of the vehicle front. The white area shows the space free of front collisions. The figure displays that for an impact point e.g. at $p_y = -0.75$ m and a model and measurement based uncertainty of $\sigma = 1.2$ m, a front collision can only be predicted with a probability of about 55%.

When a system is triggered with a front collision probability $p_{coll,front}$ greater than a threshold value of p_{thres}, the probability of a system activation event p_{event} can be determined

$$p_{event} = \iint \iint_{\Omega} f_{meas} d^2\boldsymbol{v} \mathrm{d}^2\boldsymbol{p}, \tag{15}$$

where f_{meas} is the probability density function of the position and velocity measurement and Ω is the set of all measurement values which leads to a p_{coll} greater than the threshold value of p_{thres}. A positive event is a true-positive event if there is a collision with the vehicle, whereas a false-positive event is one without a collision with the vehicle front.

Figure 7 shows the positive event probability for a threshold value of $p_{thres} = 55\%$. As shown in Fig. 6, the horizontal-axis indicates the impact point of the pedestrian. Figure 7 shows that in order to get an acceptable number of false-positive events, it is necessary to have a low standard deviation σ. For $\sigma = 1\,\text{m}$, which would be a fair performance for GNSS based localization, the false-positive rate is still about 10% for $p_y = 2\,\text{m}$, e.g. if the pedestrian crosses the vehicle front line with 1 m distance to the vehicle which is a common situation in normal traffic. Therefore, such a great false-positive probability cannot be tolerated.

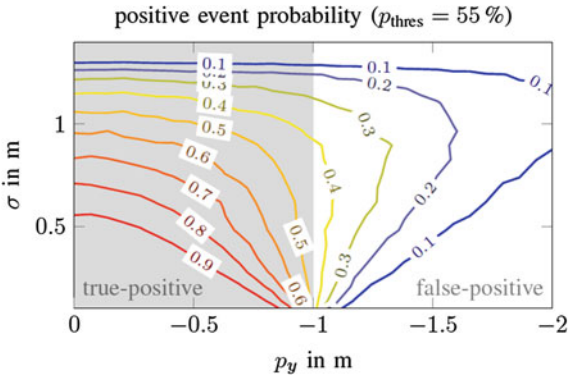

Fig. 7 False-positive and true-positive rate prediction with an assumed threshold front collision probability of $p_{coll,front} = 55\%$. The shaded area shows the true-positive rate, whereas the white area shows the predicted false-positive rate

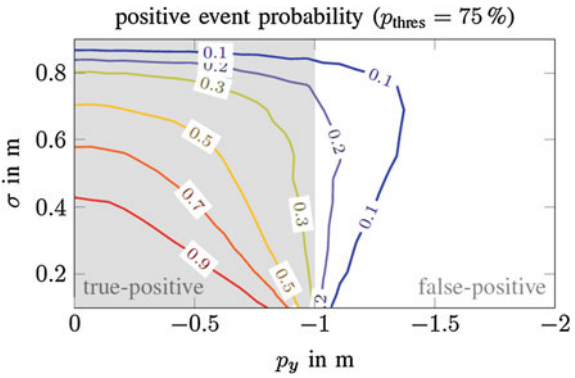

Fig. 8 False-positive and true-positive rate prediction with an assumed threshold front collision probability of $p_{coll,front} = 75\%$

Figure 8 shows the same content for a threshold of $p_{thres} = 75\%$. Assuming that a false-positive event in which a pedestrian crossing the front vehicle line with a distance of < 0.5 m is tolerable, the false-positive event probability looks better for all values of σ. However the requirement on the standard deviation σ to get a true-positive event probability by -0.75 m of 50% are a maximal value of $\sigma = 0.4$ m.

Furthermore, Figs. 7 and 8 also show impressively that a protection of pedestrians who impact the vehicle edge can only be protected if an increased false-positive rate of the system is tolerated.

The demonstrated loosely coupled localization filter with a Samsung Galaxy S3 and the u-blox M8N GNSS receiver has a standard deviation of 0.75 m ($t_{pred} = 1$ s) for the predicted pedestrian position with a neglected acceleration model $\boldsymbol{a}_{model}$. With an activation threshold of $p_{thres} = 75\%$ the true-positive rate is lower than 50%. Besides, one has to be aware that the pedestrian's acceleration model has a strong impact on the model uncertainties, which leads to a greater predictive model uncertainty $\boldsymbol{\Sigma}_{pred}(t_{TTC})$ and stronger requirements on the measurement accuracy. Research on the predictive model was made in [14, 15].

5 Discussion

In the context of situation assessment of a pedestrian protection system relevant parameters are the accuracies of the measured position, velocity and the behavior model to predict a collision and initiate the ego vehicle's best maneuver as well as the low false-positive rates with simultaneous high true-positive rates and earlier system triggering. Furthermore, a smartphone based cooperative pedestrian protection system has to have a low power consumption.

As derived in Sect. 4 the accuracy of presented localization filter has to be improved to protect pedestrians reliably. This is realizable by more accurate, especially unbiased, GNSS methods or a fusion with the ego vehicle's environment

sensors like video, radar or LiDAR. The estimated position accuracy is poor compared to the environment sensors, so that a fusion does not make sense. Whereas the estimated cooperative velocity can be used to initialize new object in the sensors' tracking filters and enables an earlier and reliable situation assessment. With the vehicle's sensors, the velocity components or tangential velocity must be derived by position measurements, which causes a settling time of the estimated velocity in the tracking filters. It has to be taken in consideration, that in a fusion approach, the problem is the object association because of the smartphone's low position accuracy and the impossible validation in the benefit scenarios, which are in particular situations where the pedestrian is visually obstructed or outside the field of view.

An advantage of the described method is, as described in Sect. 2, the availability of the IMU measurements in earth related coordinates (east, north and up), which could enable a better feature derivation for pedestrian behavior modeling.

In context of power consumption, the presented method generates small load on the communication channel to transmit the estimated position and velocity. Perhaps in a later system implementation it could be a pre-stage and a fundament of DGNSS based methods with a lower power consumption, communication load and provider of IMU's error model parameters.

6 Conclusions

In the context of smartphone based pedestrian protection systems for vehicles, this work evaluates different outdoor dead reckoning localization filters. The presented method has no restrictions of the position or the relative orientation to the walking direction of the smartphone. Thus, it allows pedestrians to carry the smartphone in trouser pockets, handbags or school bags.

Furthermore, due to the strapdown algorithm it is possible to determine the measured acceleration and rotation rate of the smartphone in earth fixed north, east and up direction with a high sampling frequency. This enables the usage for pedestrian behavior modeling and fast path prediction adaptations with V2X technology.

However, the paper shows also that further research and improvement on the used GNSS receiver and signal processing has to be done in order to ensure a better and unbiased localization accuracy. This can be effectuated by advanced GNSS techniques like computationally intensive Precise Point Positioning techniques or communication intensive DGNNS approaches. Especially DGNSS approaches between the ego vehicle and the smartphone GNSS receiver can enable better relative localization accuracy.